Multicell-to-Multicell Equalizer With Hybrid Pulsewidth Modulation and Phase-Shift Modulation

Guo Xu, *Senior Member, IEEE*, Enze Chen, Fulin Liu, Yonglu Liu, *Member, IEEE*, Wenjing Xiong, *Member, IEEE*, and Mei Su, *Member, IEEE*

***Abstract*—In this article, an any-cells-to-any-cells equalizer based on the multiwinding transformer is proposed to reduce the component number and increase the balancing speed. Every two adjacent cells only require two MOSFETs and one transformer winding to construct a buck–boost converter, and several two-cell groups construct a multiactive bridge converter, which achieves a low component number. By modulating the duty cycle and phase-shift ratio, the equalization between different cells can occur simultaneously, which achieves fast balancing speed. In addition, a current distribution strategy is designed in detail, which ensures that the balancing current of each cell is under modulation during the equalization process. Finally, a prototype, including six lithium-ion cells, is established. The experimental and comparative results verify the correctness of the theoretical analysis.**

***Index Terms*—Any-cells-to-any-cells (AC2AC) mode, fast equalizer, multiwinding transformer, phase-shifting modulation.**

I. Introduction

LITHIUM-ION batteries are widely used in energy storage systems and electric vehicles [1]. They have the advantages of high-power density, long cycle life, and low self-discharge rate. However, the terminal voltage and capacity of a lithium-ion cell are limited. In large-capacity and high-voltage applications, it is necessary to connect numerous cells in series and parallel to form a battery pack [2]. However, the energy mismatch between the serial cells will occur because of the manufacturing tolerance. In addition, repeated charging and discharging of the battery pack will aggravate the energy mismatch. Energy mismatch leads to reduced performance, shorter lifespan, and even safety hazards [3]. Hence, the battery equalizer is required to inhibit the energy mismatch between series cells to prolong the service life of the series battery pack [4].

Generally, battery equalizers are divided into dissipative and nondissipative equalizers according to balancing methods [5]. Dissipative methods use dissipative elements, such as resistors, to convert excess energy in high-voltage cells into heat for dissipation. Their advantages are simple topology, easy implementation, and mature technology. However, the mismatched energy is wasted, reducing the available capacity of the battery pack. In addition, the excess heat generated may accelerate the aging rate of nearby cells [6].

Nondissipative methods transfer the mismatched energy from the high-voltage cells to the low-voltage cells. They can achieve more efficient and rapid energy equalization. According to the balancing modes, the nondissipative methods can be divided into five categories: adjacent cell-to-cell (AC2C) [7], [8], [9], [10], [11], direct cell-to-cell (DC2C) [12], [13], [14], [15], [16], cell-to-pack (C2P) [17], [18], [19], pack-to-cell (P2C) [20], [21], [22], and any-cells-to-any-cells (AC2AC) [23], [24], [25], [26], [27], [28], [29], [30], [31], [32], [33], [34].

In the AC2C methods, energy is transferred between one pair of adjacent cells based on buck–boost and switched-capacitor converters. Phung et al. [7] proposed a balancing topology with the switched-capacitor structure, which removes all sensors but suffers from a large inrush current. To eliminate the inrush current, Yuanmao et al. [10] designed an equalizer using the quasi-resonant switched-capacitor converter. For the AC2C methods, when target cells are not adjacent, other cells are repeatedly charging and discharging, which affects the overall balancing efficiency [11]. In the DC2C method, energy is directly transferred from the highest voltage cell to the lowest to avoid repeated charging and discharging. A balancing circuit based on forward or flyback operation is proposed in [12]. It achieves fast equalization and high balancing efficiency with low complexity. To reduce the number of transformer windings, a winding-shared equalizer is proposed in [13]. However, the DC2C methods usually need a large number of switches [16]. In the C2P and P2C methods, the energy is transferred between the cell and battery pack. They make a tradeoff between cost and performance by reducing the number of switches at a slight performance sacrifice. An equalizer with time-shared flyback converter is proposed in [18]. In this circuit, energy transfer is realized through a few switches, but diodes in the path reduce

Manuscript received 23 August 2023; revised 30 October 2023; accepted 7 December 2023. Date of publication 12 December 2023; date of current version 16 February 2024. This work was supported in part by the Hunan Provincial Natural Science Foundation for Excellent Young Scholars of China under Grant 2023JJ20072, in part by the Innovation-Driven Project of Central South University under Grant 2023CXQD043, in part by the Changsha City Science and Technology Plan Project for Distinguished Young Scholars under Grant Kq2209004, in part by the Science and Technology Innovation Program of Hunan Province under Grant 2023RC3033, and in part by the National Natural Science Foundation of China under Grants 62125308 and 62192754. Recommended for publication by Associate Editor K. Basu. *(Corresponding author: Fulin Liu.)*

Guo Xu, Enze Chen, Yonglu Liu, Wenjing Xiong, and Mei Su are with the School of Automation, Central South University, Changsha 410083, China, and also with the Hunan Provincial Key Laboratory of Power Electronics Equipment and Grid, Changsha 410083, China (e-mail: xuguocsu@csu.edu.cn; chenenze@csu.edu.cn; liuyonglu@csu.edu.cn; xiongwj@csiu.edu.cn; sumeicsu@csu.edu.cn).

Fulin Liu is with the CRRC Zhuzhou Electric Locomotive Institute Company Ltd., Zhuzhou 412001, China (e-mail: liufl30@csrzic.com).

Color versions of one or more figures in this article are available at https://doi.org/10.1109/TPEL.2023.3341513.

Digital Object Identifier 10.1109/TPEL.2023.3341513

the balancing efficiency. To improve balancing efficiency, an equalizer based on an isolated bidirectional dc–dc converter is proposed in [19], which can improve efficiency through quasi-resonant operation and reduce diode count. To further improve the performance, Wei et al. [22] designed an *LCC*-based equalizer with simplified constant current control, which can effectively mitigate the inconsistency of battery strings in a fast manner. For P2C and C2P methods, the backflow energy reduces the balancing efficiency [32].

For the above four methods, the energy is only transferred between several target cells simultaneously. When all cells need to be balanced, the equalizer balances the target cells, and others need to wait for equalization. This process results in a slow balancing speed.

To solve this problem, some AC2AC topologies have been proposed. Liu et al. [29] proposed an automatic parallel resonant switched-capacitor equalizer, which achieves any cell balance simultaneously. However, $4n$ MOSFETs are required for n cells. To reduce the switch number, Liu et al. [30] designed an equalizer combining buck–boost and switched-capacitor converter, which realizes switches multiplexing; however, even though the switch is reduced, it still needs high number of magnetic components. To reduce the magnetic component number and also provide the possibility to achieve soft switching, some multiwinding transformer topologies are studied. Shang et al. [31] designed a battery equalizer based on the forward–flyback converter, which is compact and simple to control. However, when the switch is closed, there is no continuous current circuit for leakage current, and the waste of leakage inductance energy reduces the transmission power. To utilize the leakage energy, Shang et al. [32] proposed an optimized automatic equalizer with coupled half-bridge converters, which also share one magnetic core. In these topologies, the device components are reduced. However, the balancing current is dependent on the voltage difference. A low-voltage difference results in a slow balancing speed. In order to increase the balancing speed, Dam and John [33] proposed a fast cell-to-cell voltage equalizer. This method realizes the simultaneous energy equalization with a controllable balancing current between any cells through phase-shifting modulation, which achieves fast energy transfer. However, $2n$ MOSFETs and n low-frequency passive components are needed for n cells in the equalizer, resulting in high component number and large size.

To reduce the component number and also increase the balancing speed, a multiwinding transformer-based battery equalizer with pulsewidth modulation (PWM) and phase-shift modulation is proposed in this article. Compared with the automatic equalizer [29], [30], [31], [32], the switch number is the same and even lower, but the balancing current will not decrease with equalization to achieve fast balancing speed. Compared with the fast equalizer [33], the number of switches is halved, but the balancing current also will not reduce as the battery voltages approach. In the proposed topology, a group consists of two adjacent cells, two MOSFETs, and one transformer winding, which realizes the compact size and low component number. The two cells in a group form a buck–boost converter and can achieve internal equalization by adjusting the duty cycle. Each two groups can constitute a dual active bridge (DAB) converter and the cells in different groups are balanced by adjusting phase shifting. Hence, the energy path is flexible, and equalization between different cells can occur simultaneously, which increases the balancing speed.

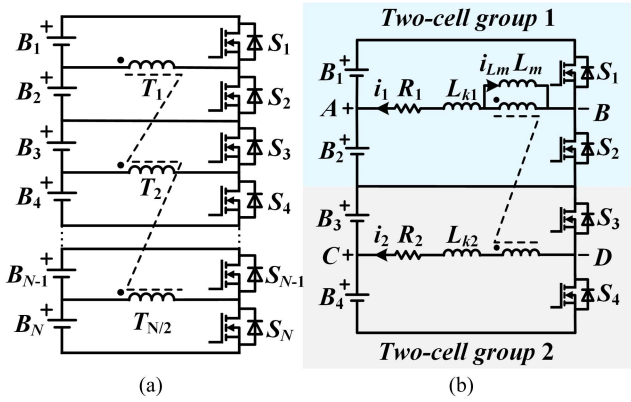

Fig. 1. Proposed equalizer. (a) Topology structure. (b) Equivalent model for four cells.

The rest of this article is organized as follows. The proposed equalizer and its operating principle are given in Section II. The operating principle and current distribution strategy of the proposed equalizer are given in Section III. In Section IV, parament designs are presented, and the experimental results are shown to verify the effectiveness of the proposed equalizer. Section V shows the comparison with the existing equalizers. Finally, Section VI concludes this article.

II. Proposed Equalizer and Operating Principle

A. Proposed Equalizer

The proposed equalizer is shown in Fig. 1(a). The battery pack, which includes n cells, is divided into $n/2$ groups, and each group consists of two adjacent cells, two MOSFETs, and one winding of the multiwinding transformer. Due to the structure of the equalizer, it cannot work properly for an odd number of cells. The magnetizing inductor is used to transfer energy between two adjacent cells in a group and the leakage inductor is used for equalization between different groups. The duty cycle of the driving signals is determined by the voltage of the cells in a group, and the phase of the driving signals is determined by the terminal voltage of different groups.

B. Operating Principles

To clearly illustrate the operation principles of the proposed equalizer, taking four cells as an example, and similar analysis can be carried out in other situations. For the convenience of analysis, the following assumptions are given.

1) The two-winding transformer can be represented by a cantilever model, as shown in Fig. 1(b). The turns number of each group of windings is the same. L_{ki}, L_m, and R_i are the leakage inductance, magnetizing inductance, and equivalent resistance of multiwinding transformer, respectively.

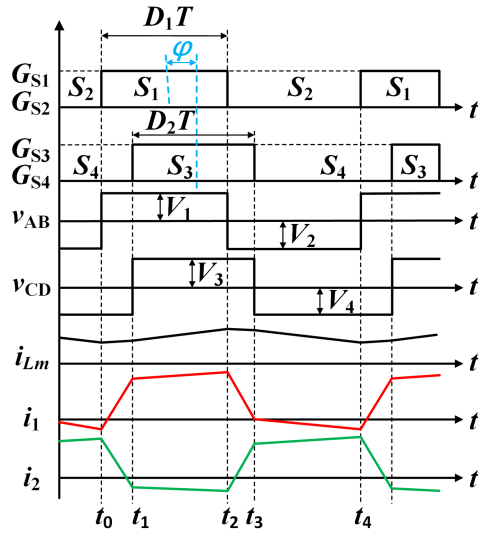

Fig. 2. Theoretical operating waveforms.

2) V_n ($n = 1, 2, 3, 4$) is the cell voltage of B_n. The initial voltage of the cell meets $V_1 > V_2 > V_3 > V_4$. In a switching cycle, the terminal voltage of the cell is constant. v_{AB} and v_{CD} are the voltages applied to the primary and secondary windings of the transformer. i_m is the current of magnetizing inductor L_m, and i_1 and i_2 are the currents of the inductors L_{k1} and L_{k2}, respectively.
3) Gs_n is the driving signal of switch S_n. D_1 is the duty cycle of S_1, D_2 is the duty cycle of S_3, switches S_1 and S_2 are complementary driven, and same are switches S_3 and S_4. φ is the angle between the center lines of the Gs_1 and Gs_3. All devices are ideal, and the parasitic capacitance of power switch is ignored.

For different battery voltage conditions, there are many combinations of duty cycle and phase-shift angle. Take the waveform in Fig. 2 as an example for analysis. In this condition, energy is transferred from B_1 to B_4. According to Fig. 2, there are four working stages in a switching cycle. Fig. 3 shows the equivalent circuit of each working stage. When studying the relationship between the transmission power of DAB converters and the phase-shift angle, the winding resistance can be ignored due to its relatively small influence on power transmission.

Stage 1 [t_0, t_1] [see Fig. 3(a)]: At t_0, S_1 and S_4 are turned ON. Under the joint action of B_1 and B_4, the current i_{Lm} increases linearly due to the negative voltage, and i_2 decreases linearly due to the positive voltage, and the following relationships are obtained:

$$i_{Lm}(t) = i_{Lm}(t_0) + \frac{V_1 - V_4}{2L_m}(t - t_0) \tag{1}$$

$$i_2(t) = i_2(t_0) + \frac{-V_1 - V_4}{L_{k1} + L_{k2}}(t - t_0). \tag{2}$$

Stage 2 [t_1, t_2] [see Fig. 3(b)]: At t_1, S_1 and S_3 are turned ON. Under the joint action of B_1 and B_3, the current i_{Lm} increases linearly due to the negative voltage, and i_2 decreases linearly due to the positive voltage, and the following relationships are obtained:

$$i_{Lm}(t) = i_{Lm}(t_1) + \frac{V_1 + V_3}{2L_m}(t - t_1) \tag{3}$$

$$i_2(t) = i_2(t_1) + \frac{-V_1 + V_3}{L_{k1} + L_{k2}}(t - t_1). \tag{4}$$

Stage 3 [t_2, t_3] [see Fig. 3(c)]: At t_2, S_2 and S_3 are turned ON. Under the joint action of B_2 and B_3, the current i_{Lm} decreases linearly due to the positive voltage, and i_2 increases linearly due to the negative voltage, and the following relationships are obtained:

$$i_{Lm}(t) = i_{Lm}(t_2) + \frac{-V_2 + V_3}{2L_m}(t - t_2) \tag{5}$$

$$i_2(t) = i_2(t_2) + \frac{V_2 + V_3}{L_{k1} + L_{k2}}(t - t_2). \tag{6}$$

Stage 4 [t_3, t_4] [see Fig. 3(d)]: At t_3, S_2 and S_4 are turned ON. Under the joint action of B_2 and B_4, the current i_{Lm} decreases linearly due to the positive voltage, and i_2 increases linearly due to the negative voltage, and the following relationships are obtained:

$$i_{Lm}(t) = i_{Lm}(t_3) + \frac{-V_2 - V_4}{2L_m}(t - t_3) \tag{7}$$

$$i_2(t) = i_2(t_3) + \frac{V_2 - V_4}{L_{k1} + L_{k2}}(t - t_3). \tag{8}$$

It can be noted that the equalization between the two adjacent cells B_1, B_2 and B_3, B_4 is automatically realized based on the buck–boost conversion during the two complementary states, and the energy equalization between the two groups is realized through the phase-shift angle.

III. Operating Mode and Current Distribution Strategy of the Proposed Equalizer

By using the superposition theorem, the cell equalization can be divided into two modes: cell equalization in a group and cell equalization between groups. Based on this analysis, the relevant current distribution strategy is formulated. Taking four cells as an example, and similar analysis can be carried out in n cells, which will be further analyzed in Section III-D.

A. Cell Equalization in a Group

Based on the assumption in Section II, when four cells are balanced, energy is transferred from the highest voltage B_1 to the lowest voltage B_4. Its equivalent circuit can be disassembled, as shown in Fig. 4.

When the target cells are in a group [B_1 and B_2 are target cells, which is shown in Fig. 4(a), or B_3 and B_4 are target cells, as shown in Fig. 4(b)], only the buck–boost converter composed of two cells and the magnetizing inductor works to achieve energy equalization. The power transmission between groups is stopped, which means that the phase-shift angle is 0°. The duty cycle of group 1 and group 2 can be adjusted by the voltage of the two cells. According to (1)–(8) and the volt-second balance

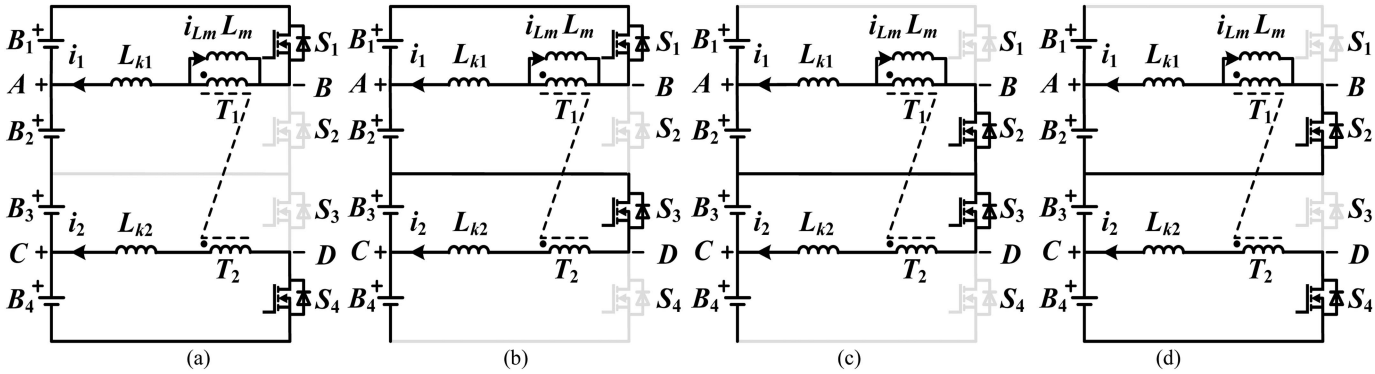

Fig. 3. Equivalent circuits of switching stages in forward mode. (a) Stage 1. (b) Stage 2. (c) Stage 3. (d) Stage 4.

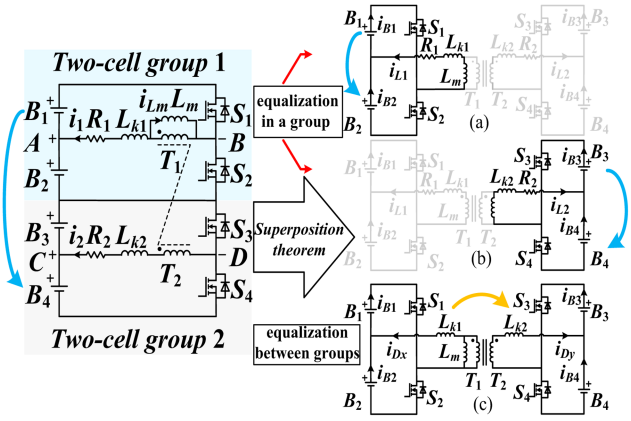

Fig. 4. Disassembly of equivalent circuit of four cells equalizer. (a) Equalization between B_1 and B_2. (b) Equalization between B_3 and B_4. (c) Equalization between groups.

of L_m, duty cycles are expressed as follows:

$$\begin{cases} D_1 = \frac{V_2+I_{L1}R}{V_1+V_2} \\ D_2 = \frac{V_4+I_{L2}R}{V_3+V_4}. \end{cases} \tag{9}$$

The magnetizing inductance of the transformer is significantly higher than the leakage inductance, so the leakage inductance can be ignored. In (9), I_{L1} and I_{L2} are the average currents flowing through the magnetizing inductor in group 1 and group 2, respectively.

B. Cell Equalization Between Groups

When the target cells are in different groups [B_1 and B_4 are in group 1 and group 2, respectively, which is shown in Fig. 4(c)], the DAB converter composed of two two-cell groups works to achieve energy equalization. It is assumed that the voltage of two cells in each group matches, and no energy is transferred between them. By applying the ampere-second principle on cell B_3, it has

$$\frac{1}{T_s}\int_0^{T_s} i_2(t) = 0 \tag{10}$$

Substituting (1)–(8) into (10), $i_2(t_0)$ is derived as (11), where $A = V_1+V_2$, $B = V_3+V_4$, $C = V_2-V_4$, $G = 2\pi f_s\,(L_{k1}+L_{k2})$, and f_s is the switching frequency.

Based on (11) shown at the bottom of the next page, the current I_{D3} flowing through cell B_3 is expressed as (12) shown at the bottom of the next page, I_{D4} is the opposite of I_{D3}, where $A = V_1+V_2$, $B = V_3+V_4$, $C = V_2-V_4$, $F = V_1+V_4$, $G = 2\pi f_s$ $(L_{k1}+L_{k2})$, and $H = 8\pi^2 f_s\,(L_{k1}+L_{k2})$.

The power transferred from group 1 to group 2 can be expressed as follows:

$$P = (-I_{D3}) \times V_3 + I_{D4} \times V_4. \tag{13}$$

The relationship between transmission power and phase-shift angle can be obtained under the condition of a fixed duty cycle, as shown in Fig. 5. In this figure, it can be obtained that the magnitude of transmission power is determined by the phase-shift angle φ, and the direction of energy transfer depends on the positive or negative phase shift. With the joint adjustment of phase-shift angle and duty cycle, the energy transfer of cells in different groups can be realized.

C. Current Distribution Strategy

According to the previous analysis, it can be found that the path of energy transmission is very flexible. To reduce the impact of polarization characteristics, the equalizer only balances the cells with the highest and lowest voltage. After collecting the voltage of each cell in real time, the balancing current is distributed according to the relationship of cell voltage. Then, the duty cycles and phase shifts can be calculated according to the circuit parameters, cells voltage, and balancing current. Finally, the switches are driven until the voltage difference between cells decreases to a certain extent Δ. The control strategy of the proposed equalizer is shown in Fig. 6.

For highest voltage cells, they need to achieve equalization by discharging, the balancing current is shown as (14). For lowest voltage cells, they need to achieve equalization by charging, the balancing current is shown as (15)

$$I_{\mathrm{dc}} = \frac{N_c}{N_{\mathrm{dc}}} \times I \tag{14}$$

$$I_c = \frac{N_{\mathrm{dc}}}{N_c} \times I \tag{15}$$

where I_{dc} is the balancing current of discharging cells, and I_c is the balancing current of charging cells. I can be adjusted

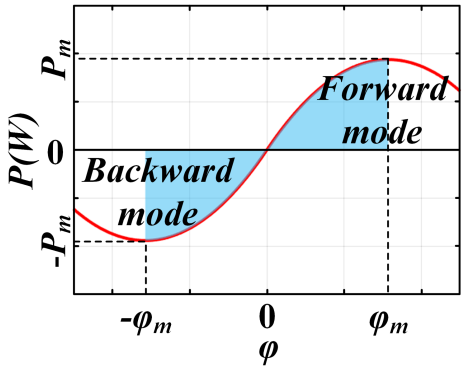

Fig. 5. Power curves versus phase-shift angle φ.

artificially according to the actual situation. N_c is the amount of charging cell. N_{dc} is the amount of discharging cell.

As shown in Fig. 4, the balancing current of four cells can be divided into two parts by applying the superposition theorem

$$I_{Bn} = I_{kn} + I_{Dn} \tag{16}$$

I_{kn} is the internal current of group i and related to I_{Li}; and I_{Dn} is the transmission current on the leakage inductor, reflecting the transferred energy between groups.

According to (16), the balancing current of four cells in two groups can be listed as follows:

$$\begin{cases} I_{B1} = I_{D1} + D_1 I_{L1} \\ I_{B2} = -I_{D2} - (1 - D_1)\, I_{L1} \\ I_{B3} = I_{D3} + D_2 I_{L2} \\ I_{B4} = -I_{D4} - (1 - D_2)\, I_{L2} \end{cases} \tag{17}$$

where $I_{D1} = -I_{D2} = I_{D12}$ and $I_{D3} = -I_{D4} = -I_{D12}$.

The specific process of calculating the duty cycles and phase shifts from the given balancing current is given as follows.

1) Combining (9) and (17), the duty cycles for each group can be obtained as follows:

$$\begin{cases} D_1 = \frac{(I_{B1} - I_{B2}) \times R + V_2}{V_1 + V_2} \\ D_2 = \frac{(I_{B3} - I_{B4}) \times R + V_4}{V_3 + V_4}. \end{cases} \tag{18}$$

2) According to the balancing current of cells, the transmission current between each two groups (I_{D12}) can be determined.
3) From (12), the phase shifts can be expressed by transmission current, and then the phase shifts can be calculated according to the constraint relationship of the phase shifts.

To clearly illustrate how the duty cycles and phase shifts are obtained, a detailed example is shown in Fig. 7. When

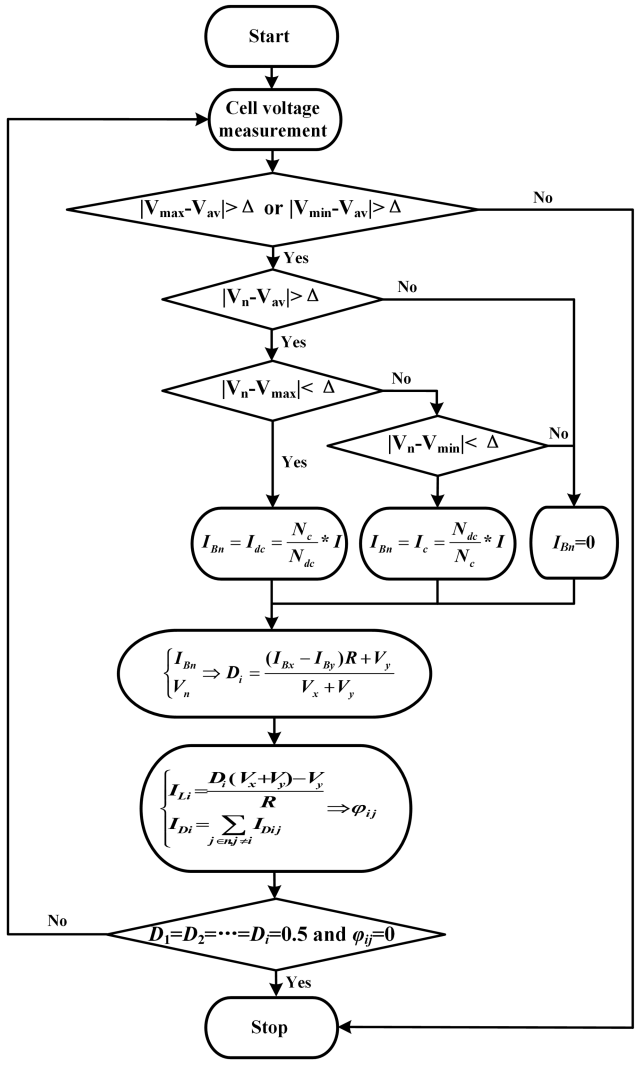

Fig. 6. Control strategy of the proposed equalizer.

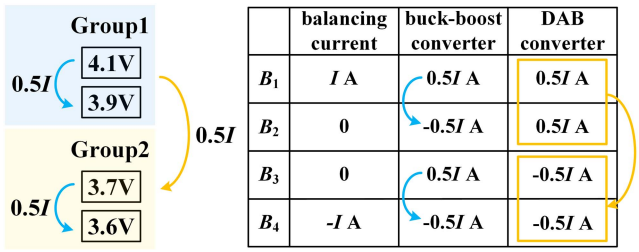

	balancing current	buck-boost converter	DAB converter
B_1	I A	0.5I A	0.5I A
B_2	0	-0.5I A	0.5I A
B_3	0	0.5I A	-0.5I A
B_4	-I A	-0.5I A	-0.5I A

Fig. 7. Energy transfer of equivalent circuit of four-cell equalizer.

$$i_2(t_0) = -\frac{A\left(2\pi D_1 - \pi D_1^2\right) + B\left(\pi D_1 D_2 + D_2\varphi - 2\pi D_2\right) - C\pi}{G} \tag{11}$$

$$I_{D3} = \frac{1}{T_s}\int_0^{D_2 T_s} i_2(t)\, dt = -\frac{A\left(\varphi^2 + \pi^2 D_1^2 + \pi^2 D_2^2 + 2\pi^2 D_1 D_2 - 2\pi D_1\varphi - 2\pi D_2\varphi - 4\pi^2 D_1^2 D_2\right)}{H} - \frac{B\left(4\pi D_2^2\varphi + 4\pi^2 D_1 D_2^2 - 4\pi^2 D_2^2\right)}{H} - \frac{C\left(4\pi^2 D_1 D_2 - 4\pi^2 D_2 + 4\pi D_2\varphi\right)}{H}. \tag{12}$$

balancing four cells, the duty cycles D_1 and D_2 can be obtained from (18). As shown in Fig. 7, the transmission current I_{D12} is $0.5I$ according to the balancing current of cells. Finally, by substituting D_1, D_2, and $I_{D12} = 0.5I$ into (12), φ_{12} is obtained.

D. Application in n Cells

When balancing n ($n \geq 4$) cells, the current distribution strategy still can be applied. The internal balance in each group is the same as the above analysis, and the duty cycles D_i can be obtained by (19) and (20), which is the extension of (9) and (18)

$$D_i = \frac{V_y + I_{Li}R}{V_x + V_y} \tag{19}$$

$$\begin{cases} I_{Bx} = I_{Dx} + D_i I_{Li} \\ I_{By} = -I_{Dy} - (1 - D_i) I_{Li} \end{cases} \tag{20}$$

where x and y are the odd and even cells in group i, respectively. I_{Li} is the average current flowing through the magnetizing inductor in buck–boost converter.

However, several groups construct a multiactive bridge (MAB) converter, which is more complex than DAB converter. As shown in Fig. 1(a), the proposed equalizer consists of $n/2$ half-bridges, which are magnetically coupled through an $n/2$ winding transformer. According to De Doncker et al. [35], the transmission power equation of DAB converter can be extended to MAB converter. Therefore, the transmission power between two-cell group i and group j of MAB converter is given by the following equation:

$$P_{ij} = \frac{V_i' V_j'}{2\pi f_s L_{ij}} \varphi_{ij} \left(1 - \frac{|\varphi_{ij}|}{\pi}\right) \tag{21}$$

where V_i' and V_j' are the dc voltages of the port; L_{ij} is the equivalent inductance between ports i and j; f_s is the switching frequency; and φ_{ij} is the phase-shift angle between two square-wave voltages at the corresponding transformer terminal.

To analyze the transmission power between ports, the delta MAB equivalent power flow model is needed, which helps in calculating the equivalent inductance (L_{ij}) between the two ports [36]. The equivalent inductance L_{ij} between group i and group j can be expressed as follows:

$$L_{ij} = L_{\sigma i} + L_{\sigma j} + L_{\sigma i} L_{\sigma j} \left(\sum_{k \neq i,j}^{n} \frac{1}{L_{\sigma k}} \right) \tag{22}$$

Combining (12) and (21), I_{Dij} can be expressed as (23) shown at the bottom of the this page, where $A = V_{i1} + V_{i2}$, $B = V_{j1} + V_{j2}$, $C = V_{i2} - V_{j2}$, $F = V_{i1} + V_{j2}$, $G = 2\pi f_s L_{ij}$, and $H = 8\pi^2 f_s L_{ij}$, and the expression of leakage inductor current of each group i is given as follows:

$$I_{D_i} = \sum_{j \in n, j \neq i} I_{D_{ij}}. \tag{24}$$

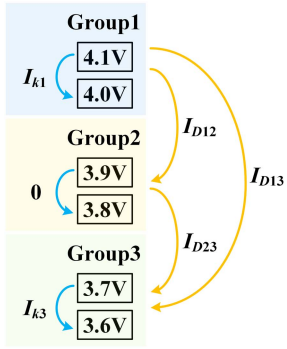

	balancing current	buck-boost converter	MAB converter
B_1	I A	$D_1 I_{L1}$ A	$I_{D12}+I_{D13}$ A
B_2	0	$-(1-D_1)I_{L1}$ A	$I_{D12}+I_{D13}$ A
B_3	0	0	$-I_{D12}+I_{D23}$ A
B_4	0	0	$-I_{D12}+I_{D23}$ A
B_5	0	$D_3 I_{L3}$ A	$-I_{D23}-I_{D13}$ A
B_6	$-I$ A	$-(1-D_3)I_{L3}$ A	$-I_{D23}-I_{D13}$ A

Fig. 8. Energy transfer of equivalent circuit of six-cell equalizer.

When balancing more than four batteries, a similar method can be used. Unfortunately, the control complexity will increase with increasing the cell count. Take six cells as an example, at this time, there are three two-cell groups and three phase shifts (φ_{12}, φ_{13}, and φ_{23}). A detailed example is shown in Fig. 8 to clearly illustrate how the duty cycles and phase shifts are obtained.

1) The duty cycles D_1, D_2, and D_3 can be obtained from (20).
2) According to (16) and (24), the transmission currents for groups where the highest voltage cell and lowest voltage cell locate can be expressed as follows:

$$\begin{cases} I_{D1} = I_{D12} + I_{D13} = I - D_1 I_{L1} \\ I_{D3} = I_{D13} + I_{D23} = -D_3 I_{L3}. \end{cases} \tag{25}$$

3) According to (23), when the duty cycle and voltage are known, $\varphi_{13} \propto I_{D13}$, $\varphi_{12} \propto I_{D12}$, and $\varphi_{23} \propto I_{D23}$. I_{L1} and I_{L3} can be obtained from (19). And then by adding the constraint relationship of $\varphi_{13} = \varphi_{12} + \varphi_{23}$, the three unknown phase shifts can be solved from three equations.

IV. Implementation and Experimental Results

The prototype of the proposed equalizer for six cells is shown in Fig. 9. Its parameter design and experimental results are introduced as follows.

A. Parameter Design

To achieve a compact structure, transformer is used as the medium of energy transmission. To avoid the bad equalization effect caused by the difference in the turn number of windings, it is necessary to ensure consistent winding turns and reasonably adjust the phase angle. The turns ratio is chosen as 4:4:4:4 to ensure equal voltage distribution and balanced power transfer

$$I_{D_{ij}} = -\frac{A\left(\varphi_{ij}^2 + \pi^2 D_i^2 + \pi^2 D_j^2 + 2\pi^2 D_i D_j - 2\pi D_i \varphi_{ij} - 4\pi^2 D_i^2 D_j - 2\pi D_j \varphi_{ij}\right)}{H} - \frac{B\left(4\pi D_j^2 \varphi_{ij} + 4\pi^2 D_i D_j^2 - 4\pi^2 D_j^2\right)}{H} - \frac{C\left(4\pi^2 D_i D_j - 4\pi^2 D_j + 4\pi D_j \varphi_{ij}\right)}{H}. \tag{23}$$

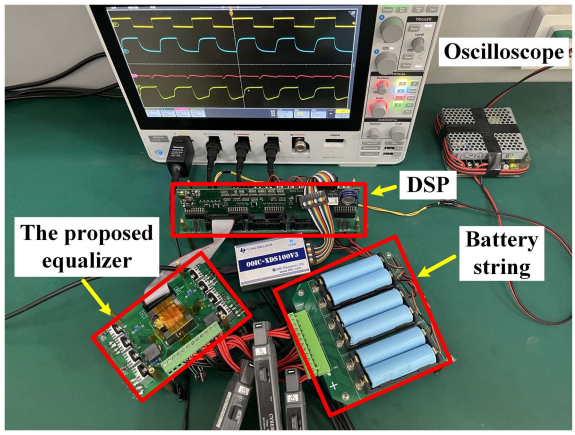

Fig. 9. Experimental prototype, including six lithium-ion cells.

across all windings. The key design parameters of equalizer include magnetizing inductance L_m and leakage inductance L_k.

For magnetizing inductance L_m, to reduce hysteresis loss and no-load loss, in any case, when the switching frequency is set to 60 kHz, the ripple current is limited to 0.3 A. The magnetizing inductance of multiwinding transformer is given as follows:

$$L_m \geq \frac{V_{\max}}{i_{\text{rip}}} \times 0.5 \times T = 111.11\,\mu\text{H}. \tag{26}$$

Although a large magnetizing inductance can reduce the ripple current in any case, the size of the transformer will increase. Hence, the magnetizing inductance is set to 120 μH.

For leakage inductance $L_{k.}$, by analyzing the power curve (shown in Fig. 5), it can be seen that when (27) is established, the maximum transmission power and maximum current are shown as (28) shown at the bottom of the this page and (29) shown at the bottom of the this page, respectively

$$\varphi_m = \frac{-B \times 2\pi D_2^2 - C \times 2\pi D_2}{A} + \pi D_1 + \pi D_2 \tag{27}$$

The voltage range of the used battery (ICR18650-26F) is 2.75–4.2 V. Considering the voltage margin, transformer parameters, and other factors, the voltage range used in this article is 3–4.1 V. When $V_1 = V_2 = 4.1$ V and $V_3 = V_4 = 3$ V, the required transmission power from DAB converter is the largest. At this time, energy transfer is stopped between cells within a group and is realized only through the phase-shift angle, that is, $D_1 = D_2 = 0.5$. Substituting $D_1 = D_2 = 0.5$ into (27)–(29), $\varphi_{\max}$, $P_{\max}$, and $I_{\max}$ are derived as follows:

$$\begin{cases} \varphi_m = \frac{(V_2V_3+V_1V_4)\pi}{(V_1+V_2)(V_3+V_4)} \\ P_{\max} = \frac{V_1V_2V_3V_4}{2(V_1+V_2)(V_3+V_4)f_sL_k} \\ I_{\max} = \frac{V_1V_2V_3V_4}{2(V_1+V_2)(V_3+V_4)^2f_sL_k}. \end{cases} \tag{30}$$

It can be seen from (24) that the transmission power increases with the decrease of leakage inductance. To achieve good conversion efficiency, set the balancing current as 0.5 A (not exceeding the maximum charging current), then $P_{\max}$ must be greater than or equal to 3 W (when the two lowest voltage cells are 3 V), so the leakage inductance is less than 8.54 μH. In addition, since the maximum current allowed for the cell is 2.6 A, the leakage inductance is greater than 1.63 μH.

To reserve a certain margin for power transmission and to avoid high currents, taking into account a variation in leakage inductance within a range of $\pm 10\%$, L_k is ultimately designed as 7.4 μH. Due to the small leakage inductance of the transformer under the parallel winding structure, the required leakage value is considered to be provided by the transformer and the external inductor. The leakage inductance of each winding is 0.4 μH and the inductance of inductor is 3.3 μH. The multiwinding transformer is composed of multiple twisted coils. The improved twisted winding method makes the windings evenly distributed and realizes a high spatial symmetry, which helps to realize consistent windings [37].

The parameter summary is shown in Table I.

TABLE I
DESIGN PARAMETERS OF THE PROPOSED EQUALIZER PROTOTYPE

Circuit Parameters	Ratings
Magnetic inductance (L_m)	120 μH
Leakage inductance (L_k)	7.4 μH
N_p:N_{s1}:N_{s2}:N_{s3}	4:4:4:4
Switching Frequency (f_s)	60 kHz
Power MOSFET	TK4R3A06PL

B. Waveforms and Conversion Efficiency

Fig. 10 shows the key waveforms for four cells. When the cells with the highest voltage and lowest voltage are in the same group, no energy needs to be transferred between two groups [such as Fig. 10(a) and (b)], and energy transfer is only realized through the duty cycle. Fig. 10(a) shows that, in the same group, one cell is discharging and one cell is charging (one-cell-to-one-cell); according to the current distribution, the distributed discharging and charging currents are 0.5 A. Fig. 10(b) shows the situation of two-cell-to-two-cell.

$$P_{\max} = \frac{BD_2}{2Af_sL_k}\left\{A^2D_1^2 + \left[V_2 + D_2V_3 + (D_2-1)V_4\right]\left[V_1 - D_2V_1 + V_2 + D_2^2V_3 + (D_2-1)D_2V_4 - 2AD_1\right]\right\} \tag{28}$$

$$I_{\max} = \frac{D_2}{2Af_sL_k}\left\{A^2D_1^2 + \left[V_2 + D_2V_3 + (D_2-1)V_4\right]\left[V_1 - D_2V_1 + V_2 + D_2^2V_3 + (D_2-1)D_2V_4 - 2AD_1\right]\right\}. \tag{29}$$

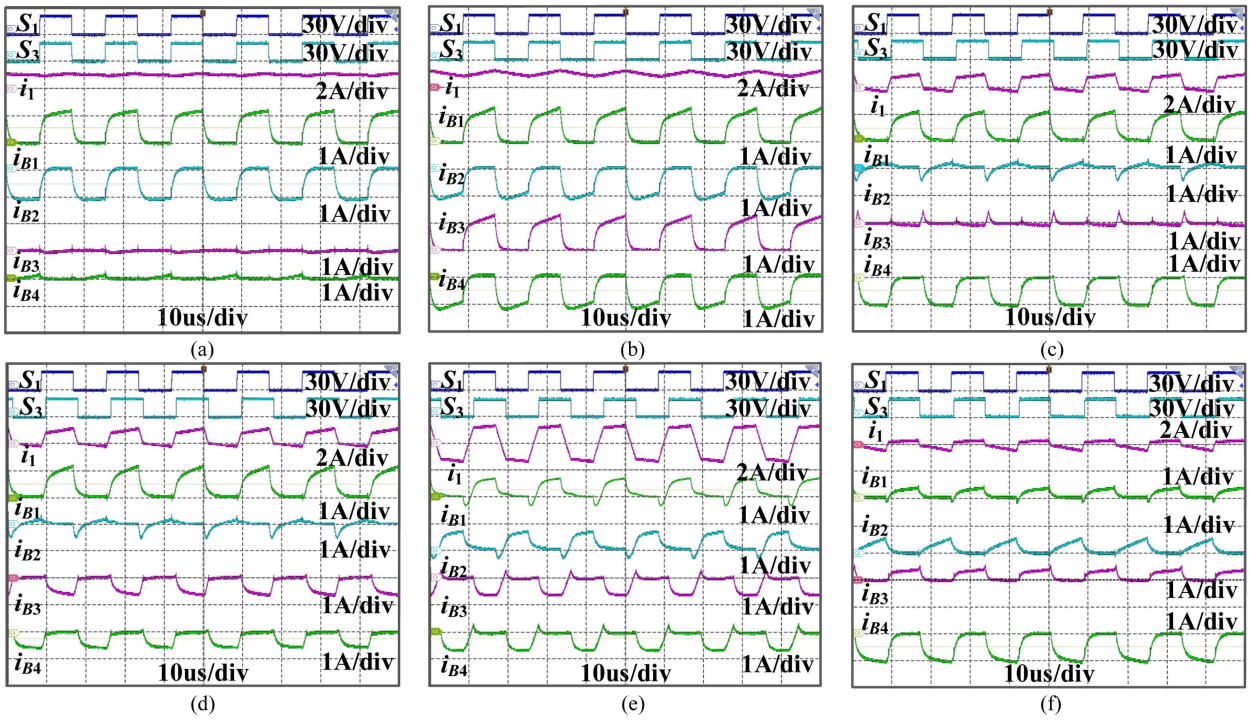

Fig. 10. Experimental waveforms for four cells. Without phase-shift angle: (a) $N_{\rm dc} = N_c = 1$ and (b) $N_{\rm dc} = N_c = 2$. With phase-shift angle: (c) $N_{\rm dc} = N_c = 1$; (d) $N_{\rm dc} = 1$ and $N_c = 2$; (e) $N_{\rm dc} = N_c = 2$; and (f) $N_{\rm dc} = 3$ and $N_c = 1$.

When voltages of the two batteries within each half-bridge structure were similar, but there was a significant voltage difference between different half-bridge structures. Energy transfer is only realized through the phase-shifting angle. Fig. 10(e) shows the situation of two-cell-to-two-cell; the distributed discharging and charging currents are 0.5 A.

When the cells with the highest voltage and lowest voltage are in different groups, energy is required to be transferred between two groups [such as Fig. 10(c), (d), and (f)]. At this time, energy transfer is realized through the combined effect of duty cycle and phase-shifting angle. Fig. 10(c) shows the situation of one-cell-to-one-cell, and the distributed discharging and charging currents are 0.5 A; Fig. 10(d) shows the situation of one-cell-to-two-cell, and the distributed discharging current is 0.5 A and the charging current is 0.25 A. There are similar waveforms in the situation of two-cell-to-one-cell; Fig. 10(f) shows the situation of three-cell-to-one-cell.

In addition, Fig. 11 shows the key waveforms for six cells. Fig. 11(a) shows waveforms in the situation of one-cell-to-one-cell, and the distributed discharging current and charging current are 0.5 A. Fig. 11(b) shows the situation of two-cell-to-one-cell. Similar results are obtained in other cases.

The above only lists the key waveform of some working modes; Figs. 10(b) and (d)–(f) and 11(b) belong to the situation of "multicell-to-multicell." The above key waveforms validate the theoretical analysis and prove the feasibility of the current distribution strategy. However, due to the limited filtering conditions employed, there are high-frequency pulse components present in the battery current waveform, which may have adverse effects on the battery's performance and lifespan.

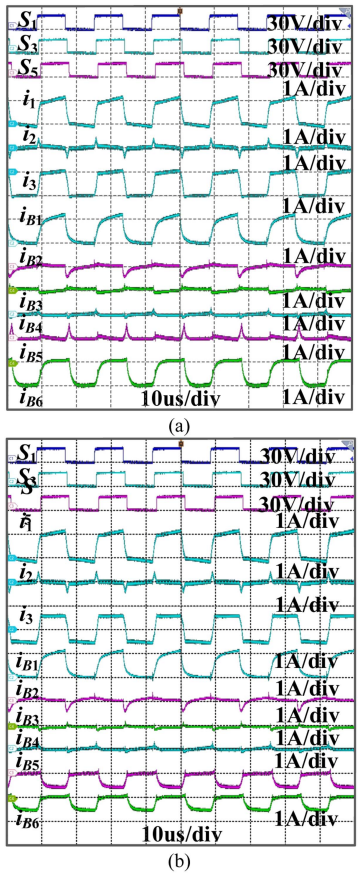

Fig. 11. Experimental waveforms for six cells. (a) $N_{\rm dc} = N_c = 1$. (b) $N_{\rm dc} = 1$ and $N_c = 2$.

TABLE II
COMPARISON OF EQUALIZER FOR BATTERY STRING CONSISTING OF *N* CELLS

Topologies		Proposed equalizer	Ref. [30]	Ref. [31]	Ref. [32]	Ref. [33]
Number of	MOSFETs	*n*	*n*	*n*	*n*	2*n*
	Windings	*n*/2	*n*/2	*n*	*n*/2	0
	Capacitors	0	/2	0	0	*n*
	Inductors	*n*	0	0	0	*n*
	sensors	*n*	0	0	0	*n*
balancing performance	Energy flow types	AC2AC	AC2AC	AC2AC	AC2AC	AC2AC
	Balancing basis	Voltage-based	Automatic	Automatic	Automatic	Voltage-based
	Balancing speed	Excellent	Good	Good	Good	Excellent
	Conversion efficiency	92	96	89.4	95	90.8

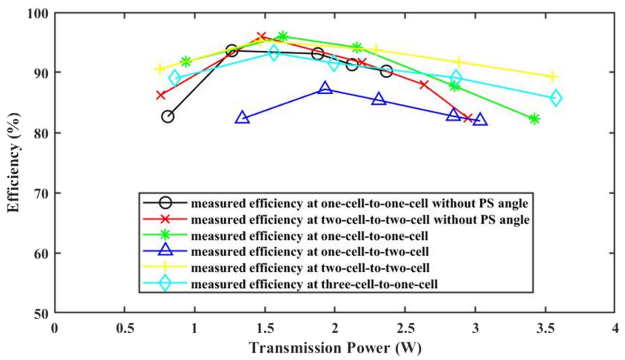

Fig. 12. Measured power conversion efficiencies.

Furthermore, the measured power conversion efficiencies for the above six modes in four cells are shown in Fig. 12. Phase-shift angle is abbreviated as PS angle. When no energy is transferred between groups, the peak efficiency for one-cell-to-one-cell is 93.6% at 1.3 W, and the peak efficiency for two-cell-to-two-cell is 96% at 1.5 W. When energy is required to be transferred between two groups, the peak efficiency for one-cell-to-one-cell, one-cell-to-two-cell, two-cell-to-two-cell, and three-cell-to-one-cell is 96% at 1.6 W, 87.2% at 1.9 W, 95.3% at 1.5 W, and 93.2% at 1.6 W, respectively. When the converter works with the situation of one-cell-to-two-cell, the circulating current and the loss of ZVS cause the low efficiency. As shown in Fig. 12, the proposed equalizer has a satisfactory conversion efficiency.

C. Balancing Results

Fig. 13(a)–(c) shows balancing results for four cells and the change of balancing current of each cell when initial conditions are $N_{\rm dc} = N_c$, $N_{\rm dc} > N_c$, and $N_{\rm dc} < N_c$, respectively.

In Fig. 13(a), the initial voltages of cells are 4.095 V, 3.906 V, 3.816 V, and 3.607 V, respectively. The equalization goes through three processes: one-cell-to-one-cell, two-cell-to-one-cell, and two-cell-to-two-cell. After 73 min, voltages become 3.834, 3.826, 3.852, and 3.851 V, and the maximum voltage gap is 26 mV. To show as many working modes as possible, the equalizer operates in one-cell-to-one-cell mode at the beginning. It would be faster if it works in two-cell-to-two-cell mode from the beginning. Fig. 13(b) shows that the initial voltages are 4.087, 3.705, 3.608, and 3.607 V. After 80 min, voltages become 3.721, 3.724, 3.738, and 3.734 V, and the maximum voltage gap is 17 mV. Fig. 13(c) shows that the initial voltages are 4.103, 4.102, 3.997, and 3.612 V. After 88 min, voltages become 3.955, 3.952, 3.95, and 3.956 V, and the maximum voltage gap is 6 mV. The slope of the equalization curve shows that the balancing current does not decrease with the decrease of voltage difference, and the magnitude of balancing current also conforms to $I_{\rm dc} = I{*}N_c/N_{\rm dc}$ and $I_c = I{*}N_{\rm dc}/N_c$ (I is set to 0.5 A). In addition, relevant experiments were also carried out in the case of six cells, and the equalization process is shown in Fig. 13(d). The initial voltages of cells are 4.09 V, 4.016 V, 3.916 V, 3.827 V, 3.722 V, and 3.618 V, respectively. The equalization goes through five processes: one-cell-to-one-cell, two-cell-to-one-cell, two-cell-to-two-cell, three-cell-to-two-cell, and three-cell-to-three-cell. After 83 min, voltages become 3.875, 3.858, 3.853, 3.853, 3.863, and 3.854 V, and the maximum voltage gap is 22 mV. The balancing results of four cells and six cells show that multiple (more than two) cells are equalized at a time. The proposed equalizer is capable of transferring energy between multiple cells, thus achieving a faster balancing speed.

V. COMPARISON WITH THE EXISTING TOPOLOGIES

The equalizer proposed in this article has the advantages of compact size, low component number, and fast balancing speed. A relatively comprehensive comparison is conducted between the proposed equalizer and several previous equalizers [30], [31], [32], [33], which are selected according to the equalization performance and application scenarios. As described in Table II, it is evaluated according to the number of components and the balancing performance, which is divided into balancing basis, balancing speed, and conversion efficiency. To make a fair

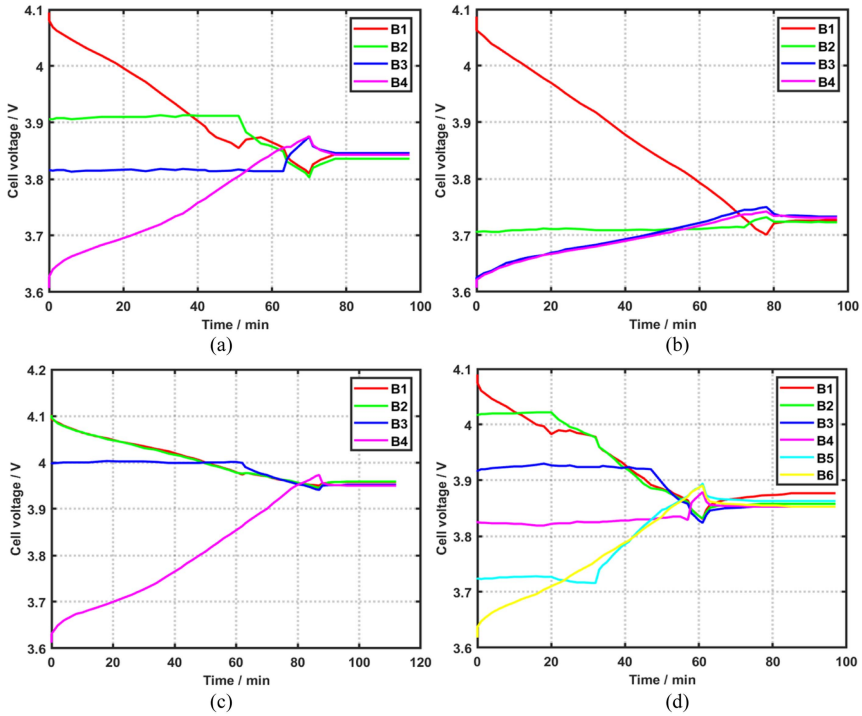

Fig. 13. Experimental results for cells with different initial voltages. For four cells: (a) $N_{\rm dc} = N_c = 2$; (b) $N_{\rm dc} = 1$ and $N_c = 3$; and (c) $N_{\rm dc} = 3$ and $N_c = 1$. For six cells: (d) $N_{\rm dc} = N_c = 3$.

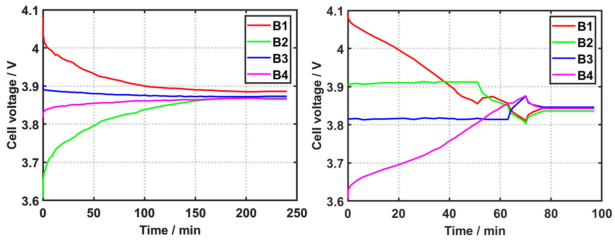

Fig. 14. Balancing results for two modulation strategies. (a) Complementary PWM. (b) Hybrid PWM and phase-shift modulation.

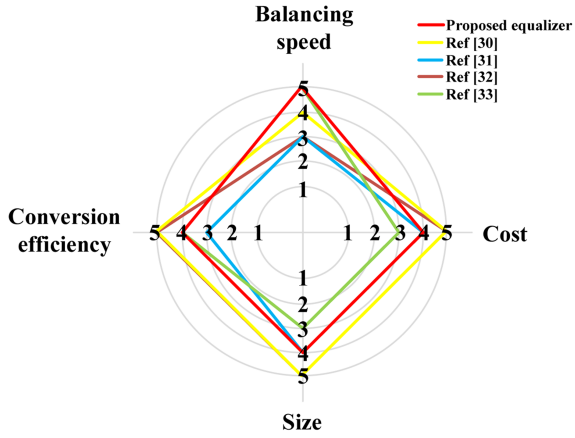

Fig. 15. Performance comparison chart.

comparison, the scores are evaluated at the same cell voltage and cell count. The balancing basis includes automatic [30], [31], [32] and voltage-based [33] mode. For automatic mode, sensors are not needed, and the balancing current is related to voltage difference. For voltage-based mode, all cell voltages are sensed to keep the required balancing current. The balancing speed of a battery equalizer depends on the balancing current and the method of energy transfer. In Fig. 14, the balancing results of the equalizer using complementary PWM and hybrid PWM and phase-shift modulation under similar voltage differentials are compared. In the equalizer using complementary PWM, after 200 min, the maximum voltage difference is reduced from 474 to 17 mV. In the equalizer using hybrid PWM and phase-shift modulation, after 73 min, the maximum voltage difference is reduced from 488 to 26 mV. The comparison revealed that the proposed equalizer achieved the equalization of cells with similar voltage differentials in a shorter time. In addition, compared with the fast equalizers [33], the proposed equalizer requires fewer magnetic components, which provides cost advantages. The conversion efficiency is defined as the ratio of output and input powers. The input power is the total power of the discharging cells, and the output power is the total power of the charging cells. The maximum efficiency value obtained during the entire power transfer process is taken as the basis for comparison. The use of phase-shift modulation will correspondingly bring about the effect of circulating current, which will have a certain impact on the efficiency.

To intuitively show the performance of each equalizer, a comparison diagram, as shown in Fig. 15, is drawn based on the above comparison results. Each parameter is fuzzed into five

fuzzy scales in which "1," "2," "3," "4," and "5" represent the worst, worse, neutral, good, and best performance, respectively.

Compared with automatic equalizers [30], [31], [32], the balancing current of the proposed equalizer in this article is controllable and does not decrease as the voltage difference between the cells reduces. To achieve a faster balancing speed, the proposed equalizer makes certain tradeoffs in terms of control complexity and the requirement for voltage sensors. Compared with the fast equalizer [33], the proposed equalizer reduces the number of switches by half to achieve less cost and size.

VI. Conclusion

A multiwinding transformer-based battery equalizer with PWM and phase-shift modulation is proposed in this article, which has the advantages of low component number and fast balancing speed. By two cells with respective MOSFET sharing one transformer winding, the number of components is reduced. By adopting the PWM modulation and phase-shifting modulation, the internal balance of each group and the balance between each group are realized, respectively, and the energy can be transferred between any cells simultaneously to achieve fast balancing speed. The experimental results verify the theoretical analysis and system feasibility of the method and show that the equalizer can realize fast and accurate AC2AC equalization, and the balancing currents of each cell are adjustable during the equalization process. As the number of batteries increases, the complexity of controlling and constructing multiwinding transformers becomes more demanding.

References

[1] L. Liu et al., "A low-cost multiwinding transformer balancing topology for retired series-connected battery string," *IEEE Trans. Power Electron.*, vol. 36, no. 5, pp. 4931–4936, May 2021.

[2] D.-H. Kim, M.-J. Kim, and B.-K. Lee, "An integrated battery charger with high power density and efficiency for electric vehicles," *IEEE Trans. Power Electron.*, vol. 32, no. 6, pp. 4553–4565, Jun. 2017.

[3] K. Liu, Z. Wei, C. Zhang, Y. Shang, R. Teodorescu, and Q.-L. Han, "Towards long lifetime battery: AI-based manufacturing and management," *IEEE/CAA J. Automatica Sinica*, vol. 9, no. 7, pp. 1139–1165, Jul. 2022.

[4] M. Uno and K. Tanaka, "Single-switch multioutput charger using voltage multiplier for series-connected lithium-ion battery/supercapacitor equalization," *IEEE Trans. Ind. Electron.*, vol. 60, no. 8, pp. 3227–3239, Aug. 2013.

[5] D. F. Frost and D. A. Howey, "Completely decentralized active balancing battery management system," *IEEE Trans. Power Electron.*, vol. 33, no. 1, pp. 729–738, Jan. 2018.

[6] S.-W. Lee, K.-M. Lee, Y.-G. Choi, and B. Kang, "Modularized design of active charge equalizer for Li-ion battery pack," *IEEE Trans. Ind. Electron.*, vol. 65, no. 11, pp. 8697–8706, Nov. 2018.

[7] T. H. Phung, A. Collet, and J.-C. Crebier, "An optimized topology for next-to-next balancing of series-connected lithium-ion cells," *IEEE Trans. Power Electron.*, vol. 29, no. 9, pp. 4603–4613, Sep. 2014.

[8] S. Wang, S. Yang, W. Yang, and Y. Wang, "A new kind of balancing circuit with multiple equalization modes for serially connected battery pack," *IEEE Trans. Ind. Electron.*, vol. 68, no. 3, pp. 2142–2150, Mar. 2021.

[9] C. Pascual and P. T. Krein, "Switched capacitor system for automatic series battery equalization," in *Proc. Appl. Power Electron. Conf.*, 1997, pp. 848–854.

[10] Y. Yuanmao, K. W. E. Cheng, and Y. P. B. Yeung, "Zero-current switching switched-capacitor zero-voltage-gap automatic equalization system for series battery string," *IEEE Trans. Power Electron.*, vol. 27, no. 7, pp. 3234–3242, Jul. 2012.

[11] Z. Zhang, H. Gui, D.-J. Gu, Y. Yang, and X. Ren, "A hierarchical active balancing architecture for lithium-ion batteries," *IEEE Trans. Power Electron.*, vol. 32, no. 4, pp. 2757–2768, Apr. 2017.

[12] Y. Chen, X. Liu, Y. Cui, J. Zou, and S. Yang, "A MultiWinding transformer cell-to-cell active equalization method for lithium-ion batteries with reduced number of driving circuits," *IEEE Trans. Power Electron.*, vol. 31, no. 7, pp. 4916–4929, Jul. 2016.

[13] S.-H. Park, K.-B. Park, H.-S. Kim, G.-W. Moon, and M.-J. Youn, "Single-magnetic cell-to-cell charge equalization converter with reduced number of transformer windings," *IEEE Trans. Power Electron.*, vol. 27, no. 6, pp. 2900–2911, Jun. 2012.

[14] K.-M. Lee, S.-W. Lee, Y.-G. Choi, and B. Kang, "Active balancing of Li-ion battery cells using transformer as energy carrier," *IEEE Trans. Ind. Electron.*, vol. 64, no. 2, pp. 1251–1257, Feb. 2017.

[15] P.-H. La and S.-J. Choi, "Direct cell-to-cell equalizer for series battery string using switch-matrix single-capacitor equalizer and optimal pairing algorithm," *IEEE Trans. Power Electron.*, vol. 37, no. 7, pp. 8625–8639, Jul. 2022.

[16] Y. Yu, R. Saasaa, A. A. Khan, and W. Eberle, "A series resonant energy storage cell voltage balancing circuit," *IEEE J. Emerg. Sel. Topics Power Electron.*, vol. 8, no. 3, pp. 3151–3161, Sep. 2020.

[17] M. Uno and K. Tanaka, "Single-switch cell voltage equalizer using multistacked buck-boost converters operating in discontinuous conduction mode for series-connected energy storage cells," *IEEE Trans. Veh. Technol.*, vol. 60, no. 8, pp. 3635–3645, Oct. 2011.

[18] A. M. Imtiaz and F. H. Khan, "'Time shared flyback converter' based regenerative cell balancing technique for series connected Li-ion battery strings," *IEEE Trans. Power Electron.*, vol. 28, no. 12, pp. 5960–5975, Dec. 2013.

[19] J. Lu, Y. Wang, and X. Li, "Isolated bidirectional DC–DC converter with quasi-resonant zero-voltage switching for battery charge equalization," *IEEE Trans. Power Electron.*, vol. 34, no. 5, pp. 4388–4406, May 2019.

[20] M. Uno and A. Kukita, "Double-switch equalizer using parallel- or series-parallel-resonant inverter and voltage multiplier for series-connected supercapacitors," *IEEE Trans. Power Electron.*, vol. 29, no. 2, pp. 812–828, Feb. 2014.

[21] M. Arias, J. Sebastián, M. M. Hernando, U. Viscarret, and I. Gil, "Practical application of the wave-trap concept in battery–cell equalizers," *IEEE Trans. Power Electron.*, vol. 30, no. 10, pp. 5616–5631, Oct. 2015.

[22] Z. Wei, F. Peng, and H. Wang, "An LCC-based string-to-cell battery equalizer with simplified constant current control," *IEEE Trans. Power Electron.*, vol. 37, no. 2, pp. 1816–1827, Feb. 2022.

[23] Y. Shang, C. Zhang, N. Cui, and J. M. Guerrero, "A cell-to-cell battery equalizer with zero-current switching and zero-voltage gap based on quasi-resonant LC converter and boost converter," *IEEE Trans. Power Electron.*, vol. 30, no. 7, pp. 3731–3747, Jul. 2015.

[24] Y. Ye, K. W. E. Cheng, Y. C. Fong, X. Xue, and J. Lin, "Topology, modeling, and design of switched-capacitor-based cell balancing systems and their balancing exploration," *IEEE Trans. Power Electron.*, vol. 32, no. 6, pp. 4444–4454, Jun. 2017.

[25] Y. Shang, N. Cui, B. Duan, and C. Zhang, "Analysis and optimization of star-structured switched-capacitor equalizers for series-connected battery strings," *IEEE Trans. Power Electron.*, vol. 33, no. 11, pp. 9631–9646, Nov. 2018.

[26] Y. Shang, C. Zhang, N. Cui, and C. C. Mi, "A delta-structured switched-capacitor equalizer for series-connected battery strings," *IEEE Trans. Power Electron.*, vol. 34, no. 1, pp. 452–461, Jan. 2019.

[27] L. Liu, W. Sun, P. Han, R. Mai, Z. He, and W. Li, "Design of zero-current parallel-switched-capacitor voltage equalizer for battery strings," in *Proc. IEEE Appl. Power Electron. Conf. Expo.*, 2019, pp. 3180–3183.

[28] S. K. Dam and V. John, "Low-frequency selection switch based cell-to-cell battery voltage equalizer with reduced switch count," *IEEE Trans. Ind. Appl.*, vol. 57, no. 4, pp. 3842–3851, Jul./Aug. 2021.

[29] L. Liu, R. Mai, B. Xu, W. Sun, W. Zhou, and Z. He, "Design of parallel resonant switched-capacitor equalizer for series-connected battery strings," *IEEE Trans. Power Electron.*, vol. 36, no. 8, pp. 9160–9169, Aug. 2021.

[30] K. Liu, Z. Yang, X. Tang, and W. Cao, "Automotive battery equalizers based on joint switched-capacitor and buck-boost converters," *IEEE Trans. Veh. Technol.*, vol. 69, no. 11, pp. 12716–12724, Nov. 2020.

[31] Y. Shang, B. Xia, C. Zhang, N. Cui, J. Yang, and C. C. Mi, "An automatic equalizer based on forward–flyback converter for series-connected battery strings," *IEEE Trans. Ind. Electron.*, vol. 64, no. 7, pp. 5380–5391, Jul. 2017.

[32] Y. Shang, N. Cui, and C. Zhang, "An optimized any-cell-to-any-cell equalizer based on coupled half-bridge converters for series-connected battery strings," *IEEE Trans. Power Electron.*, vol. 34, no. 9, pp. 8831–8841, Sep. 2019.

[33] S. K. Dam and V. John, "A modular fast cell-to-cell battery voltage equalizer," *IEEE Trans. Power Electron.*, vol. 35, no. 9, pp. 9443–9461, Sep. 2020.
[34] F. Liu, R. Zou, and Y. Liu, "An any-cell-to-any-cell battery equalizer based on half-bridge LC converter," *IEEE Trans. Power Electron.*, vol. 38, no. 4, pp. 4218–4223, Apr. 2023.
[35] R. W. A. A. De Doncker, D. M. Divan, and M. H. Kheraluwala, "A three-phase soft-switched high-power-density DC/DC converter for high-power applications," *IEEE Trans. Ind. Appl.*, vol. 27, no. 1, pp. 63–73, Jan./Feb. 1991.
[36] S. Bandyopadhyay, P. Purgat, Z. Qin, and P. Bauer, "A multiactive bridge converter with inherently decoupled power flows," *IEEE Trans. Power Electron.*, vol. 36, no. 2, pp. 2231–2245, Feb. 2021.
[37] R. Zou, F. Liu, Y. Liu, G. Xu, and F. Liu, "An LLC-based battery equalizer with inherent current limitation," *IEEE Trans. Power Electron.*, vol. 37, no. 2, pp. 1828–1840, Feb. 2022.

Guo Xu (Senior Member, IEEE) received the B.S. degree in electrical engineering and automation and the Ph.D. degree from the Beijing Institute of Technology, Beijing, China, in 2012 and 2018, respectively.

From 2016 to 2017, he was a Visiting Student with the Center for Power Electronics System, Virginia Polytechnic Institute and State University, Blacksburg, VA, USA. Since 2018, he has been with the School of Automation, Central South University, Changsha, China, where he is currently an Associate Professor. His research interests include modeling and control of power electronics' converters, high-efficiency power conversion, and magnetic integration in power converters.

Enze Chen was born in Zhejiang, China, in 2000. He received the B.S. degree in electrical engineering and automation from the Changsha University of Science and Technology, Changsha, China, in 2022. He is currently working toward the M.S. degree in electrical engineering with Central South University, Changsha, China.

His research interests include battery equalizers and dc/dc converters.

Fulin Liu was born in Shandong, China, in 1994. He received the B.S., M.S., and Ph.D. degrees from Central South University, Changsha, China, in 2016, 2019, and 2023, respectively.

He is currently working with CRRC Zhuzhou Electric Locomotive Institute Company Ltd., Zhuzhou, China. His research interests include battery equalizers, three-phase bidirectional ac/dc converters, and bidirectional dc/dc converters.

Yonglu Liu (Member, IEEE) was born in Chongqing, China, in 1989. He received the B.S., M.S., and Ph.D. degrees in electrical engineering from Central South University, Changsha, China, in 2012, 2015, and 2017, respectively.

He is currently an Associate Professor with the School of Automation, Central South University. His research interests include power electronics and renewable energy power conversion systems.

Wenjing Xiong (Member, IEEE) was born in Hunan, China, in 1991. She received the B.S. degree in automation and the Ph.D. degree in control science and engineering from Central South University, Changsha, China, in 2012 and 2017, respectively.

She is currently an Associate Professor with the School of Automation, Central South University, China. Her research interests include matrix converter, ac/dc converter, and multilevel converters.

Mei Su (Member, IEEE) was born in Hunan, China, in 1967. She received the B.S., M.S., and Ph.D. degrees from the School of Automation, Central South University, Changsha, China, in 1989, 1992, and 2005, respectively.

She has been a Full Professor with the School of Automation, Central South University. She is currently an Associate Editor for IEEE TRANSACTIONS ON POWER ELECTRONICS. Her research interests include matrix converter, adjustable speed drives, and wind energy conversion system.